Numerical Simulation of Warm-air Drying of Mexican Softwood (*Pinus pseudostrobus*): An Empirical and Mechanistic Approach

S. Sandoval-Torres,[a,*] E. Hernández-Bautista,[a] J. Rodríguez-Ramírez,[a] and A. Carrillo Parra[b]

[a]Instituto Politécnico Nacional, CIIDIR Unidad Oaxaca,
Hornos No. 1003, Col. Noche Buena, Santa Cruz Xoxocotlan, Oaxaca, México
[b]Facultad de Ciencias Forestales, Universidad Autónoma de Nuevo León,
Carr. Nal. Km. 145, 67700 P.O. Box 041 Linares, Nuevo León, México

Original scientific paper
Received: May 22, 2013
Accepted: August 4, 2013

In this work, the numerical simulation of Mexican softwood (*Pinus pseudostrobus*) drying is presented by solving a phenomenological model. The model was developed by considering the heat and mass balance in the representative elementary volume, which involves the solid, liquid and gas phases. We solved a system of partial differential equations by numerical factorization in COMSOL multiphysics 3.5a©. Three primary variables were solved: the moisture content, the temperature, and the dry-air mass. The numerical results were compared against both experimental data and a semi-empirical model (Characteristic Drying Curve) previously published. The warm-air drying of Mexican softwood was simulated on a one-dimensional basis by considering two experimental conditions: air flow temperature at 60 and 80 ºC. Relative humidity was not controlled in the tunnel dryer. Simulated drying kinetics showed good agreement with the experimental data.

Key words:
Warm-air drying, phenomenological model, multi-physics, numerical simulation, *Pinus pseudostrobus* wood

Introduction

The evacuation of water in biological materials like wood is a very complex phenomenon, since it involves coupled mechanisms occurring simultaneously during the drying.[1]

Wood is extremely non-homogeneous, and its structural and chemical variability is reflected in its transport properties such as permeability, capillary behavior, thermal conductivity, and the diffusion of bound water.[2] There are four key relationships in the structure of wood cell walls: (i) aggregation of cellulose, lignin, and hemicelluloses molecules to form larger structures; (ii) arrangement of these structures to conform a multilayered cell wall; (iii) different concentrations of cellulose, hemicelluloses, and lignin within the cell wall and the intercellular region; and (iv) specialization of cell walls, such as interconnecting pits. Since the polymers that constitute wood each have different sorption isotherms, and thermal conductivity, wood is in fact a composite material where the overall behavior is a result of the properties of the individual components and their arrangement in the wood structure.[3] In addition, the transport phenomena in wood can be a very difficult task if we consider this arrangement.

Water in wood can exist as either absorbed (free water) in the cell lumens and intercellular spaces or as adsorbed (bound water) within the cell walls. When wood dries, liquid water first evaporates from the lumens and intercellular spaces. Two domains exist in wood, the first one called the capillary region, and the second called the hygroscopic region. Both regions are limited by the fiber saturation point of wood. The fiber saturation point (FSP) is defined as the moisture content at which all the absorbed water has been removed but at which the cell walls are still fully saturated. This occurs at a moisture content of approximately 25 to 35 %. In softwoods, it is adequate to presume the fiber saturation point to be 30 % moisture content.[4,5]

Moisture flow in wood is a very complex phenomenon, since different wood-water relations exist. The flow paths through softwoods are shown in Fig. (1).

During drying, as the liquid water is being removed from the capillaries, at the same time it is replaced by air and water vapor. This gas flow (air+water vapor) in porous media is transported through the cell wall by adsorption, diffusion, and desorption (Fig. 2).

*Author for correspondence: ssandovalt@ipn.mx

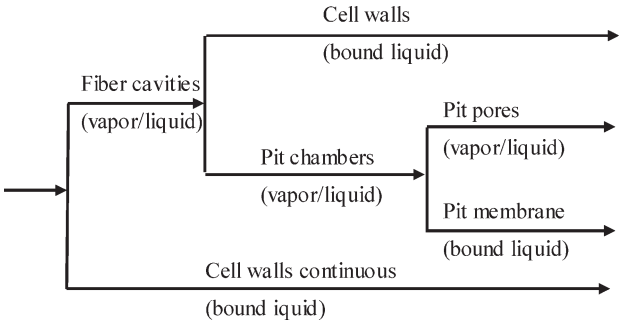

Fig. 1 – *Flow paths through softwoods*[2]

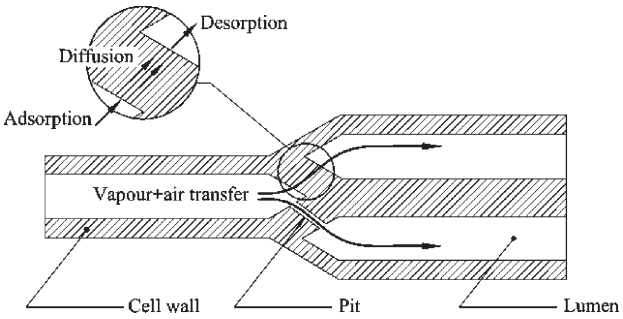

Fig. 2 – *Water vapor and air transport in wood*[6]

During drying, the evaporative plane divides the board into two regions: a wet region within the core and a much drier region in the outer wedge. In the drier region, moisture is assumed to exist as bound water and water vapor. The bound water is removed from the solid matrix by desorption and subsequently transported by diffusion. Bound water will be in local thermodynamic equilibrium with the water vapor at the local temperature. The drying process stops when the equilibrium moisture content is reached.

In past years, several models have been proposed. The most advanced models are called "phenomenological models". The phenomenological models take into account the thermodynamic fundamentals of transfers in porous media, and consider the contribution of each phase.[7] Some phenomenological models have been modified to offer more efficient solutions,[8] these models involve coupled balances by considering the representative average volume concept (REV).

Several publications dealing with wood drying exist in literature. Many oriented to European woods, as pine (*Pinus maritime*) and oak (*Quercus pedonculae*),[9–12] nevertheless, the lack of drying models for Mexican softwoods (endemic species) limits improvements of this operation, since one of the handicaps of the Mexican forest industry is poor technological development.[13]

The aim of this work was to develop and solve, on a one-dimensional basis, a phenomenological model to simulate drying kinetics and moisture distribution during warm-air convective drying of Mexican softwood (*Pinus pseudotrobus*). The phenomenological model was compared versus a semi-empirical model previously published.[14] Modeling the drying process will provide useful information to optimize the drying operation. The present work is a first attempt with Mexican softwoods.

Materials and methods

The drying trials were carried out in a dryer tunnel. A uni-variate statistical design was used where temperature was controlled at 2 levels. The air drying temperature was controlled at 60 and 80 °C. The air velocity was constant in all trials (2.5 m s^{-1}), and the relative humidity was not controlled but it was logged. The drying flow (humid air) was heated by two electrical resistances of 20 Ω, (2.4 kW) and controlled by a PID system. Both the air temperature and the relative humidity were measured by a Vaisala sensor. Two thermocouples were installed inside the wood, the first one near the surface, and the second in the middle (Fig. 3). The weight of the sample was measured by a load cell (COLE-PARMER, range 0–11.34 kg, 0.1 % accuracy). All data were logged by using a data acquisition system (Texas National Instruments) through the LabVIEW software.

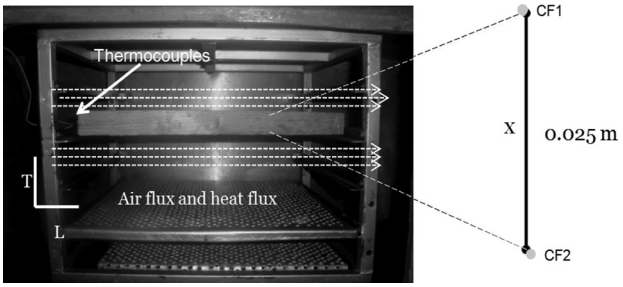

Fig. 3 – *Experimental setup in the drying tunnel and geometry*

Fresh wood boards were taken at random from the sawmill "*Pueblos Mancomunados de la sierra Norte*", located in the community of Macuilxochitl Artigas Carranza, near Oaxaca City – Mexico. The samples were 25 cm long, 15 cm wide, and 2.54 cm thick. The fresh boards were immediately sprayed using a disperser and covered with a waterproof plastic. The wood samples were immediately stored at 0 °C in the refrigerator to prevent degradation. For each experiment, two samples of fresh wood were used. The edges were sealed with red silicone in order to ensure one-directional (1-D) transport. Each trial lasted approximately 70 hours. All drying conditions were duplicated.

Mathematical formulation

Drying characteristic curve DCC

From experimental data, we have deduced a model based on the method of drying characteristic curve (DCC), to simulate the drying kinetics. The model was developed from the analysis of the reduced drying rate and the identification of stages, by considering a drying rate of reference. This model establishes moisture transport mechanisms depending on the reduced moisture content exclusively. This model was the first part of our research work. The two proposed equations were eq. 1 and eq. 2:

$$CH_r = CH_{r2}; CH(t) = CHE + \left(CH_{cr} - CHE\right) \cdot \cdot \left[\left(CH_{r2} + \frac{d}{c}\right)\exp\left(\frac{cV_{ref}}{CH_{cr} - CHE}(t - t_2)\right) - \frac{d}{c}\right] \quad (1)$$

$$CH = CH_{r0}; CH(t) = CHE - \frac{1}{b}\left(CH_{cr} - CHE\right) \cdot \cdot \ln\left[\exp\left(-b\, CH_{r0}\right) + \frac{a\, b\, V_{ref}\, t}{CH_{cr} - CHE}\right] \quad (2)$$

Where the parameters *a*, *b*, *c*, and *d* were estimated by using the expression:

$$SE_i = \left[\sum_{i=1}^{n}\left(\frac{CH_{\exp} - CH_{\mathrm{mod}}}{CH_{\exp}}\right)\right]_i \quad (3)$$

More details about the characteristic drying curve have been previously published.[14]

Phenomenological model

As a second part of our investigation, a phenomenological formulation was numerically solved by taking into account a multiphase perspective.[7,15] We assumed the moisture transport is done mainly in the thickness direction (1D), and then the model's geometry is represented in COMSOL by a straight line (Fig. 3), where the line represents the thickness of wood.

The three primary variables to solve were: the moisture content (W); the intrinsic density of air (ρ_a) and the temperature (T).

The moisture transfer (eq. 4) is a more elaborate version of the diffusive model; it considers the transport of liquid water, water vapor and bound water. The separation of phases and the constitutive relations include the contribution of each of the phases. The flow of free water is assumed to follow a particular behavior described by Darcy's law; therefore the mass average velocity is given by eq. 5. Capillary pressure causes the liquid to move towards the drying surface. Several works have shown the gravity term is very small and therefore negligible.[16,17]

$$\frac{\partial W}{\partial t} = -\nabla \cdot \left\{\frac{1}{\rho_s}\left(\overline{\rho}_l \overline{\mathbf{v}}_l + \overline{\rho}_v \overline{\mathbf{v}}_v^g + J_b\right)\right\} \quad (4)$$

$$\rho_l \mathbf{v}_l = \rho_l \frac{\mathbf{Kk}_{rl}}{\mu_l}\nabla \cdot P_c - \rho_l \frac{\mathbf{Kk}_{rl}}{\mu_l}\nabla \cdot P_g^g \quad (5)$$

The transport of water vapor and dry air can be described by the combination of Fick's and Darcy's law. Therefore, we can represent the transport of gaseous phase (water vapor and dry-air) by the eqs. 4, 6, 7 and 8. The flow of dry air is similar to water vapor expression, which has two terms (eq. 7), the pressure gradients and the concentration gradients. Gas pressure can be considered since the gaseous mixture is strongly affected by temperature, and the wood ultrastructure suffers geometric changes in the matrix, so small capillaries generate important pressure at the liquid-gas interface.

The liquid transport is also affected by the liquid concentration in wood, because water in high concentration zones can move to the low concentration zones; this movement has a strong relationship with both saturation and capillary pressure.

The flow equation for dry-air (eq. 8) represents the convective flow of gas-phase that results from total gaseous pressure. It considers the contribution of the pressure gradients present in the thickness of wood, in fact this expression is an advective-diffusive model, and explains the gas transport by a linear addition of advection calculated by Darcy's law and ordinary diffusion using Fick's law. The contribution of dry-air can be computed since we consider Raoult's law for the gaseous mix. Thus, for the air mass conservation and the gaseous entities, we have:

$$\frac{\partial}{\partial t}\left(\overline{\rho}_a\right) + \nabla \cdot \left(\overline{\rho}_a^g \overline{\mathbf{v}}_a\right) = 0 \quad (6)$$

$$\overline{\rho}_v^g \overline{\mathbf{v}}_v = -\overline{\rho}_v^g \frac{\mathbf{Kk}_{rg}}{\mu_g} \cdot \nabla \overline{P}_g^g - \overline{\rho}_g^g \mathbf{D}_{eff} \nabla\left(\frac{\overline{\rho}_v^g}{\overline{\rho}_g^g}\right) \quad (7)$$

$$\overline{\rho}_a^g \overline{\mathbf{v}}_a = -\overline{\rho}_a^g \frac{\mathbf{Kk}_{rg}}{\mu_g} \cdot \nabla \overline{P}_g^g - \overline{\rho}_g^g \mathbf{D}_{eff} \nabla\left(\frac{\overline{\rho}_a^g}{\overline{\rho}_g^g}\right) \quad (8)$$

Within a homogeneous phase (gas, liquid, or solid) the mass transfer of a molecular species occurs primarily by diffusion. Wood is a non-homogeneous material; in this case we could take into account the gas pressure gradient. Gas-phase diffusion in porous media is an important factor within transport in wood, since water vapor must be evacuated during drying. Several models have been used to

quantify gas diffusion processes in porous media. Fick's law is the most popular approach to gas diffusion due to its simplicity. However, physically, Fick's law applies to gas diffusion in open spaces, not within porous media, and therefore, we considered the Darcy´s law.

The transport mechanism of bound water is described by eq. 9. This expression takes into account two mechanisms; the bound water content gradients (Dufour effect) and temperature gradients (Soret effect). It is well accepted that temperature gradients could be a secondary driving force for the mass transfer.

$$J_b = -\rho_s \mathbf{D_b} \cdot \nabla W_b - \rho_s \underset{bt}{D} \nabla T \tag{9}$$

The water activity (% RH) of the gaseous phase at the FSP is unity, and therefore no vapor-pressure gradients are possible above the FSP. The model considers the bound water transport depends on both temperature and moisture content. Moreover, gas-phase transport (ρ_g) occurs due to the development of total pressure gradients inside the board.

Stamm[18] has suggested that the relative vapor pressure, or relative humidity, at FSP saturation is about 0.995, whereas Skaar[19] takes a value for relative humidity of 0.99 at the FSP point. This depression of relative humidity at FSP saturation is presumed to be caused by both condensation of water at the lumen ends and the tiny micropores and/or cavities in the cell wall. In this work we have used the isotherms published in Rodriguez *et al*.,[20] which were obtained from Mexican softwood.

Bound water will be in local thermodynamic equilibrium with the water vapor at the local temperature.

Eq. 10 represents the energy balance for drying. It considers heat conduction, the energy contribution of each phase, as well as the enthalpy changes due to the phase change.

$$\rho C_p \frac{\partial T}{\partial t} + \Delta h_{vap} \overline{m}_{lv} + \Delta h_{sorp} \overline{m}_{bv} + \\ + \left(C_{pl}\rho_l \mathbf{v}_l + C_{pb}\rho_b \mathbf{v}_b + C_{pv}\rho_v \mathbf{v}_v + C_{pa}\rho_a \mathbf{v}_a\right) \cdot \\ \cdot \nabla T = \nabla\left(\lambda \nabla T\right) \tag{10}$$

Boundary conditions

The surface fluxes are calculated using the heat- and mass-transfer coefficients and the corresponding potentials. Continuity of moisture transfer must occur at the board surface. As mentioned above, Fig. 3 shows the model's geometry. There are two boundary conditions CF1 and CF2, they are initially considered at the same temperature, these boundary conditions represent the experimental conditions affecting the wood surface.

Eq. 11 represents the outward flow of vapor water leaving the material. This is the boundary condition for the moisture content conservation equation.

$$\mathbf{J_w} \cdot \hat{\mathbf{n}} = \overline{\mathbf{m}}_{\mathbf{lv}} = k_m c M_v \ln\left(\frac{1 - x_{v_\infty}}{1 - x_v}\right) \tag{11}$$

To solve the dry-air mass equation, a Neumann boundary condition is applied; because it is a mass flux.

For the energy equation, since the heat over the surface is removed by the airflow, eq. 12 takes into account the convective heat transfer (air flow at 2.5 m s^{-1}) and the heat flux needed to remove moisture (desorption heat). To consider the real situation during drying, we have computed the coefficients of heat and mass transfer from experimental data obtained in our configuration.

$$\mathbf{J_e} \cdot \hat{\mathbf{n}} = \mathbf{q} + \Delta h_v \overline{\mathbf{m}}_{\mathbf{lv}} = \\ = h\left(T - T_\infty\right) + \Delta h_v k_m c M_v \ln\left(\frac{1 - x_{v_\infty}}{1 - x_v}\right) \tag{12}$$

It is important to note that the air velocity used yielded heat and mass transfer coefficients of 21 W m^{-2} K^{-1} and 0.021 m s^{-1}, respectively. To simulate the drying kinetics it was necessary to have the thermo-physical properties for this Mexican softwood (*Pinus pseudostrobus*). This Mexican conifer wood has been poorly studied. However, we have used the thermo-physical properties of similar conifers (similar in density). We assume an important variability of thermo-physics properties between softwoods. Some of the properties used are shown in Table 1. The isotherms used in this work correspond to *Pinus pseudostrobus* wood previously published.[20]

Model implementation in COMSOL

The model was solved using the nonsymmetric-pattern multifrontal method and direct LU factorization of the sparse matrix. It employs the COLAMD (column approximate minimum degree ordering) and AMD approximate minimum degree preordering algorithms to permute the columns so that the fill-in is minimized. The model has been implemented in COMSOL Multiphysics 3.5a©.

To solve the mass conservation equation (moisture and air) we used the PDE module, and to solve the energy conservation equation, the heat transport module.

Table 1 – *Thermo-physical properties of softwoods*

Property	Relation to value	Reference
Porosity	$\varepsilon = 0.66$	
Fiber saturation point	$W_{psf} = 0.30$	Fuentes-Salinas[21]
Absolute permeability	$\hat{\mathbf{E}} = 1 \cdot 10^{-17}$	Raji *et al*[10]
Specific heat of solid	$C_{ps} = 1400$	Hernández y Puiggali[22]
Relative gas permeability	$\mathbf{k}_{rg} = 1 + (2S - 3)S^2$	Perré y Turner[1]
Relative liquid permeability	$\mathbf{k}_{rl} = S^3$	Perré y Turner[1]
Capillary pressure	$P_c = 1.4 \cdot 10^6 S^{-0.63}$	Kang y Chung[23]
Bound liquid diffusivity	$\mathbf{D_b} = 2 \cdot 10^{-13} \exp\left[5.46W + 2.54 \cdot 10^{-2} T\right]$	Colakoglium[24]
Air-vapor diffusivity	$\mathbf{D}_{av} = 2.2 \cdot 10^{-5} \left(\frac{101325}{P_g^g}\right)\left(\frac{T}{273.15}\right)^{1.81}$	Baronasa *et al*[25]
Effective diffusivity	$\mathbf{D}_{eff} = k_{rg}\mathbf{D}_{av}\left(1 \cdot 10^{-3}\right)$	Wook *et al*[26]
Sorption isotherms	$W_{eq}(T, Hr) = \frac{X_m \cdot C \cdot K \cdot Hr}{(1 - K \cdot Hr)(1 + C \cdot K \cdot Hr - K \cdot Hr)}$ $C = 0.0064 \cdot T^2 - 0.5807 \cdot T + 21.962$ $Xm = -0.0006 \cdot T + 0.0883$ $K = 0.0022 \cdot T + 0.695$	Sandoval-Torres *et al*.[20]
Thermal conductivity	$\lambda = 0.137 + 0.386W$	Hernández y Puiggali[22]

To solve the highly non-linear equations system, the mesh used consisted of 125 elements, with a relative and absolute tolerance of 0.1 and 0.01, respectively. Relative tolerance needs to be scalar, and is used to control any unknown variables. Absolute tolerance allows the singling out of individual variables. The system of equations was solved using a computer with processor Intel Core Duo 1.83 GHz. Solution in COMSOL multiphysics for both drying at 60 °C and 80 °C took 2.8 seconds.

Results

In order to explain and simplify the results, in this paper we considered two cases: 1) Constant air-flow temperature at 60 °C, initial drying temperature of 25 °C with initial moisture content of wood of 96 % (wet basis), and 2) Constant air-flow temperature at 80 °C, initial drying temperature of 25 °C and initial moisture content of wood of 102 % (wet basis).

Fig. 4 depicts the experimental data and the simulated drying kinetics of both approaches: the drying characteristic curve and the phenomenological approach. Fig. 4 includes an axis on the right side to plot the temperature profiles in both the center and on the surface of the boards. The average moisture content curve in Fig. 4 shows a constant rate period up to a drying time of around 1 h (3600 s).

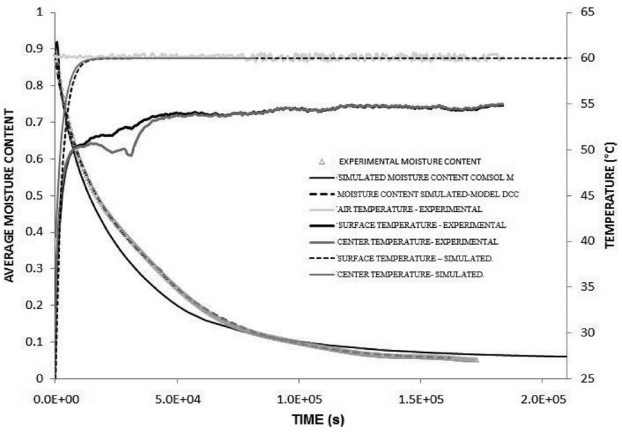

Fig. 4 – *Drying kinetics and average temperature evolution – Drying flow at 60 °C*

At high moisture content (at the beginning), the capillary flow is most important. In fact, during the constant rate period, the primary mechanism of liquid migration is due to capillary action. In the first hours of drying, the gas-liquid interaction in the pores develops a capillary pressure which depends on several factors; nevertheless, in this work we

considered capillary pressure as a function of saturation. A deviation near the FSP can be explained by high variation of thermal properties, capillary pressure, permeability and shrinkage. Furthermore, the FSP was 0.3, which is a value proposed for conifers.

The heat supplied by the external airflow is used primarily to transform free water into vapor. For drying at 60 °C, experimental temperature on the surface of wood reaches 55 °C while in our numerical simulations the surface was heated until 60 °C; this fact can be due to differences between relative humidity (RH) values of both the real and the theoretical conditions. In the real conditions (experimental), RH was not controlled, and in the numerical solution, RH was considered constant (30 %).

According to Nijdam,[5] the surface temperature often approaches an asymptotic value well below the external air temperature, when drying sapwood under high-temperature conditions. In our experiments, we applied moderate temperatures, and it can be observed that the asymptotic value was never reached. To improve the temperature evolution it should be important to consider a more appropriate thermal conductivity for *Pinus pseudostrobus*.

Fig. 5 displays the drying kinetics and temperature evolution of drying at 80 °C. It can be observed that the numerical drying kinetics and the experimental results are in good agreement. Simulation tracks correctly the moisture loss during drying. As in the first case, the numerical solution of temperature shows a difference versus the experimental data, explained by the uncontrolled water vapor in the atmosphere; The RH in the air flow was tuned by the mass flux evacuated from the board, while in numerical simulation was considered constant.

In Fig. 5, the gradient of temperature is more important between the surface and the middle of the board; near the wood surface, the air flow was at 80 ºC, and the gas-phase convective flow over the wood surface removed water vapor at a higher drying rate compared to drying at 60 ºC, then equilibrium moisture content was reached in a shorter time.

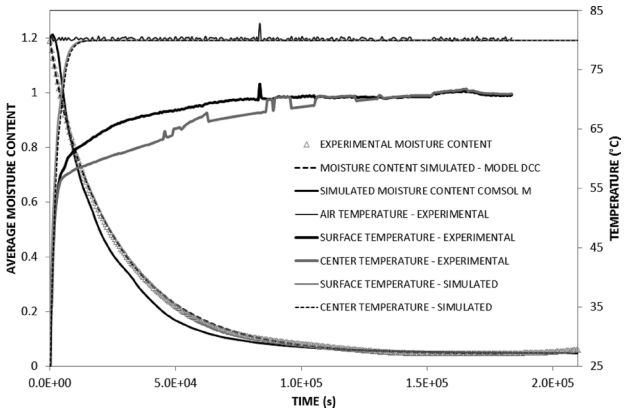

Fig. 5 – *Drying kinetics and average temperature evolution – Drying flow at 80 °C*

Fig. 6 shows the moisture distribution along the thickness of wood piece and its evolution at intervals of 1000 s for drying at 60 ºC. As liquid water is removed, it is replaced by the gaseous phase. A fluctuation in the parable of moisture content is due to the phase transition, because the capillary phase ends and the hygroscopic phase begins. This fluctuation mainly depends on both the relative permeability function and the capillary pressure terms, whose influence directly affects the liquid water transport. Mathematically, the saturation term softens the parables with squared functions.

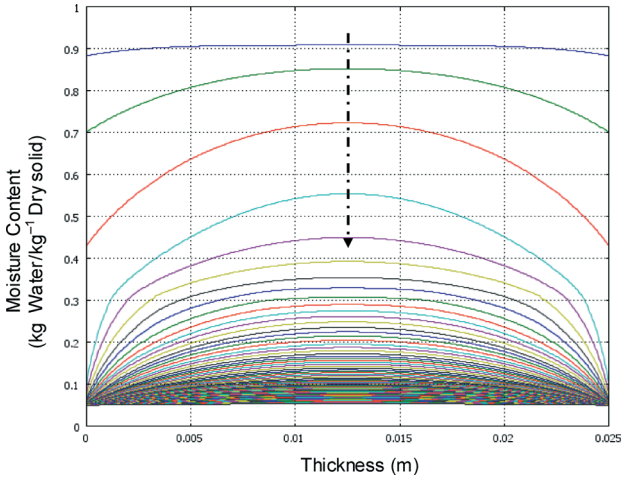

Fig. 6 – *Moisture distributions through the thickness of wood every 1000 s. Drying at 60 °C.*

In Figs. 7a and 7b, we present the moisture content profiles for the two different conditions of drying. Both figures display the numerical results until 4000 s (the beginning of drying). At 80 °C moisture loss is evidently more intense than at 60 °C, and in the first seconds of drying, the moisture distribution is almost flat.

In Fig. 8, the distribution of water vapor along wood thickness is displayed. The water vapor pressure increases during drying, because the gaseous mixture replaces the evacuated liquid water, and this gas phase depends mainly on temperature. Our model assumes that the relative humidity of the gas at the fiber-saturation point is unity, and therefore no vapor-pressure gradients are possible above the fiber-saturation point. For this reason, the water activity expression is considered only below the fiber-saturation point (FSP). We know that the gas mixture is a combination of water vapor and dry air, and this is described by Dalton's law, which establishes that the pressure of a mixture of non-reactive gases is equal to the sum of each of them. The solution of water vapor expression is a parabolic

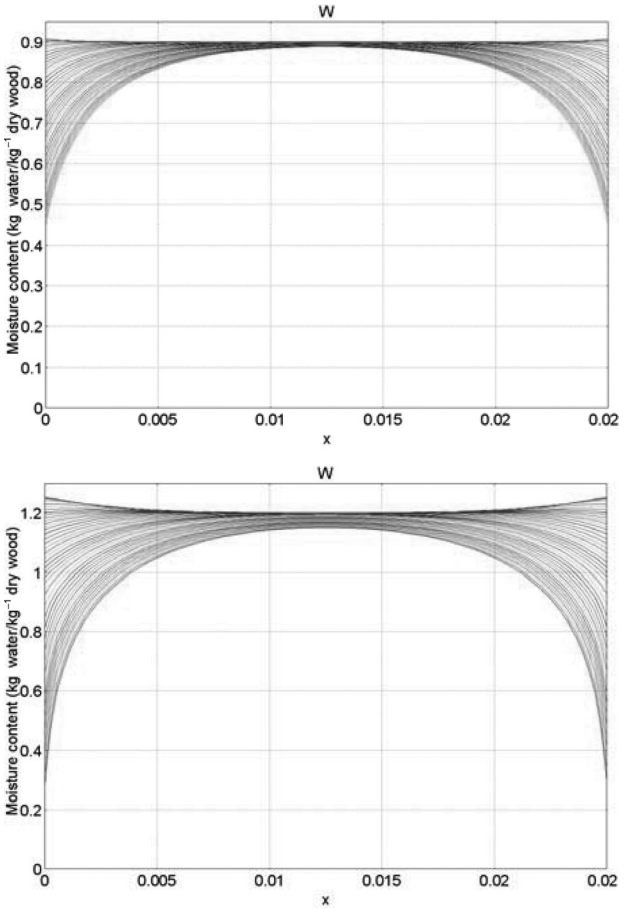

Fig. 7 – *a) Moisture content profiles every 100 s until 4000 s – drying at 50 °C. W_{ini} = 0.9; b) Moisture content profiles every 100 s until 4000 s – drying at 80 °C. W_{ini} = 1.2.*

function. The vapor pressure evolution indicates this behavior during drying.

The third unknown in our system of equations is the dry-air (ρ_a). In Fig. 9, the dry air distribution inside the wood is shown.

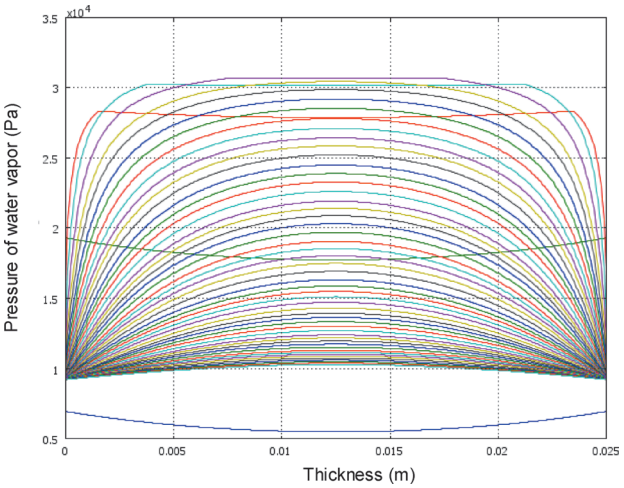

Fig. 8 – *Vapor pressure distribution through the thickness of wood every 1000 s*

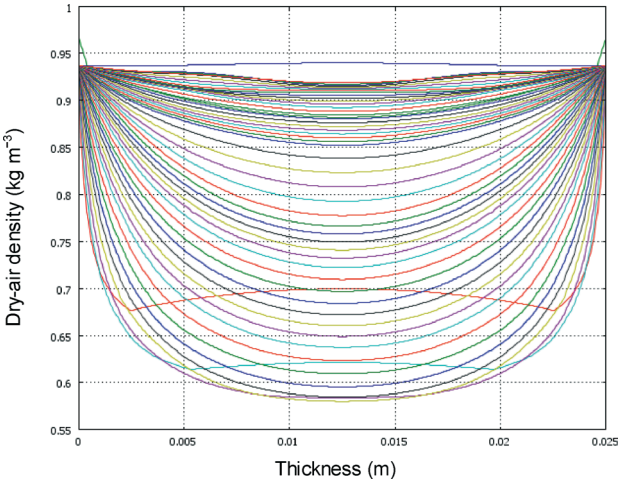

Fig. 9 – *Dry-air density distribution through the thickness every 4000 s*

It would be interesting to see the moisture losses at different depths of the board. In Fig. 10, we present these curves, which show how moisture in wood surface firstly reaches equilibrium. It is convenient to say that in this work we used sapwood only. Moisture losses at different depths of the wood are well simulated. Some regions (layers of wood at the surface) reach equilibrium moisture content faster, which is consistent with drying physics.

The evaporative front recedes and the velocity with which it recedes is well observed. Fig. 10 shows that the moisture distribution develops different drying rates, and at the surface, the moisture decrease is greater than in the internal layers of wood.

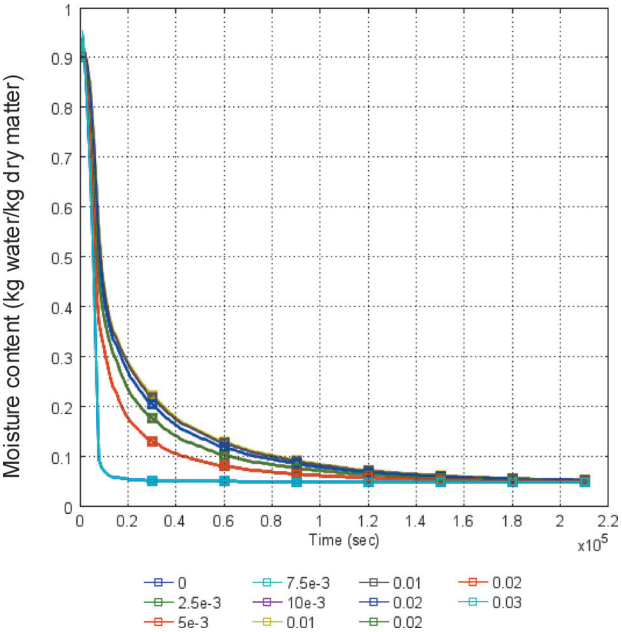

Fig. 10 – *Moisture content evolution at different depths (every 2.5 mm) of wood. Drying at 60 °C.*

Conclusion

Drying kinetics for warm-air drying of Mexican softwood were simulated. The simulations tracked the drop in the average-board moisture content with time. A better fit was obtained using the drying characteristic curve method (CCS) previously published, since its parameters were fitted from experimental data.

In this work, many of the transport properties needed for the phenomenological model correspond to similar softwood species, so the variations in the numerical results of the phenomenological model could be diminished if their thermo-physical properties were experimentally obtained. Nevertheless, the drying kinetics and the moisture profiles are well described, and the drying physics explained.

To enhance the phenomenological model, the thermal and transport properties must be experimentally calculated for this wood species (*Pinus pseudostrobus)*. In fact, nowadays more complex models are necessary, since they provide more information about the transport phenomena. This should not be surprising, since complexity means information that is so random and irregular that it cannot be compressed into description or definition.

The numerical results describe correctly the drying behavior of *Pinus psedostrobus* wood, and moisture distribution. The model displays a strong reliance of the physical properties of wood. This is the first time a drying simulation for Mexican softwood was accomplished by considering a mechanistic approach. The one-dimensional model can capture the major drying processes and is fast to run.

Notation

C – constant of Gab
c – molar concentration (mol m^{-3})
C_p – specific heat (J kg^{-1} K^{-1})
C_{pa} – specific heat of air (J kg^{-1} K^{-1})
C_{pb} – specific heat of bound water (J kg^{-1} K^{-1})
C_{pl} – specific heat of liquid water (J kg^{-1} K^{-1})
C_{pv} – specific heat of vapor (J kg^{-1} K^{-1})
$\boldsymbol{D}_{av}$ – air vapor diffusivity (m^2 s^{-1})
$\boldsymbol{D}_b$ – bound water diffusivity (m^2 s^{-1})
$\boldsymbol{D}_{bt}$ – bound water de thermo- diffusivity (m^2 s^{-1})
$\boldsymbol{D}_{eff}$ – effective diffusivity (m^2 s^{-1})
H_r – relative humidity
h – heat transfer coefficient (W m^{-2} K^{-1})
$\boldsymbol{J}_b$ – bound water flux (kg m^{-2} s^{-1})
$\boldsymbol{J}_w$ – liquid flux (kg m^{-2} s^{-1})
$\boldsymbol{J}_e$ – energy flux (J m^{-2} s^{-1})
$\boldsymbol{K}$ – absolute permeability of wood (m^2)
K_m – mass transfer coefficient (m s^{-1})
$\boldsymbol{K}_{rg}$ – relative gas permeability
$\boldsymbol{K}_{rl}$ – relative liquid permeability
Mv – molecular weight of vapour (mol kg^{-1} mol^{-1})
$\boldsymbol{n}$ – normal vector (m)
m_{bv} – rate of mass transfer liquid to bound water (kg s^{-1})
m_{lv} – rate of mass transfer liquid to vapour water (kg s^{-1})
P_{atm} – atmospheric pressure (Pa)
P_c – capillary pressure (Pa)
P_g^g – gas pressure (Pa)
R – universal gas constant (J mol^{-1} K^{-1})
t – time (s)
T – temperature (K)
T_∞ – drying temperature (K)
$\boldsymbol{v}_a$ – air velocity (m s^{-1})
$\boldsymbol{v}_l$ – liquid phase velocity (m s^{-1})
$\boldsymbol{v}_v$ – vapour velocity (m s^{-1})
W – moisture content (kg water kg^{-1} drying solid)
W_b – moisture content of bound water (kg water kg^{-1} drying solid)
W_{eq} – equilibrium moisture content (kg water kg^{-1} drying solid)
$W_{inicial}$ – initial moisture content (kg water kg^{-1} drying solid)
W_{psf} – fiber saturation point (kg water kg^{-1} drying solid)
X_m – GAB's constant
x_v – molar fraction of vapour at exchange surface (mol mol^{-1})
$x_{v\infty}$ – molar fraction of vapour at in the air (mol mol^{-1})
Δh_{sorp} – differential heat of sorption (J kg^{-1})
Δh_{vap} – differential heat of vaporization (J kg^{-1})
ε – porosity (m^3 m^{-3})
$\boldsymbol{\lambda}$ – thermal conductivity (W m^{-2} K^{-1})
μ_g – vapor viscosity (Pa s)
μ_l – viscosity of water (Pa s)
r_a – air density (kg m^{-3})
r_b – bound water density (kg m^{-3})
r_l – liquid density (kg m^{-3})
r_s – solid density (kg m^{-3})
r_v – vapor density (kg m^{-3})

References

1. *Perré, P., Turner, I. W.,*AIChE J. **52** (2006) 3109.
2. *Siau, J. F.,* Transport Processes in Wood: Springer Series in Wood Science (1984).
3. *McDonald, A. G.,* Constituents in wood, in: Encyclopedia of Materials: Science and Technology, Elsevier Science (2001).
4. *Walker, J. C. F.,* Water in wood, in: Primary Wood Processing, 2nd edition, The Netherlands, Springer (2010).
5. *Nijdam, J. J., Langrish, T. A. G., Keey, R. B.,* Chem. Eng. Sci. **55** (2000) 3585.
6. *Krabbenhøft, K.,* PhD Thesis, Technical University of Denmark, Denmark (2003).
7. *Whitaker, S.,* Advances in Heat Transfer **13** (1977) 119.

8. *Perré, P.,* COST action E15, Advances in the drying of wood (1999).
9. *Fernandez, M., Howell, J.,* Drying technol. **15** (1997) 2343.
10. *Raji, S., Jannot, Y., Lagière, P., Puiggali, J.,* Constr. Build. Mater. **23** (2009) 3189.
11. *Turner, I., Puiggali, J., Jomaa, W,* Trans IChemE. **76** (1998) 193.
12. *Perré, P., Turner, I.,* Drying Technol. **17** (1999) 1273.
13. *Forster, H., René, A., Argüelles, A., Aguilar, N., Kaatz, S.,* Opciones Y Barreras De Mercado Para Madera Aserrada De Michoacán, Oaxaca, Guerrero, Campeche Y Quintana Roo, Mexico, Report to Forest Trends, Mexico (2004).
14. *Hernández-Bautista, E., Sandoval-Torres, S., Rodríguez-Ramírez, J., Velasco-Cruz, O. A.,* Bois et forêts des tropiques **306** (2010).
15. *Perré, P., Turner, I. W.,* AIChE J. **52** (2001) 3109.
16. *Plumb, O., Prat, M.,* Drying **92** (1992) 397.
17. *Turner, I., Rousset, P., Rémond, R., Perré, P.,*Int. J. Heat Mass Transfer **53** (2010) 715.
18. *Stamm, A. J.,* Wood Sci. **4** (1971) 114.
19. *Skaar, C.,* Wood-Water Relations, Berlin (1988) 35–42.
20. *Rodriguez-Ramirez, J., S. Sandoval-Torres, S., L. Mendez-Lagunas,L., Parra, A. C.,* Forestry Studies in China **13** (2011) 285.
21. *Fuentes-Salinas, M.,* Revista Chapingo Serie Ciencia Forestales y del Ambiente **6** (2000) 79.
22. *Hernández, J. M., Puiggali, J. R.,* Int. J. Chem. Eng. **34** (1994) 339.
23. *Kang, W., Chung, W. Y.,* The Japan Wood Res. Soc. **55** (2009) 91.
24. *Colakoglium, M. H.,* J. Appl. Sci. **9** (2009) 4091.
25. *Baronasa, R., Ivanauskasa, F., Juodeikienėc, I., Kajalavičiusc, A.,* Modelling and Control **6** (2001) 3.
26. *Wook, K., Chung, W. Y., Eom, C. D., Yeo, H.,* The Japan Wood Res. Soc. **54** (1977) 267.